Theory of double internal bremsstrahlung during electron-capture decay

Robert L. Intemann
Department of Physics, Temple University, Philadelphia, Pennsylvania 19122
(Received 21 December 1994)

The theory of double internal bremsstrahlung during an allowed electron-capture transition is developed in an approximation in which the atomic electron is treated nonrelativistically but the effects of the nuclear Coulomb field are fully included. For capture from the K shell detailed results are obtained for the intensity distribution of the two photons as a function of the photons' energies and relative angle of emission. Numerical results are presented for the distribution of the sum of the photon energies for ^{37}Ar and ^{55}Fe and compared with available experimental data. It is found that the inclusion of Coulomb effects results in a substantial reduction in the intensity of the energy spectrum of the photons and improves quantitative agreement with the experimental data for ^{37}Ar. However, for ^{55}Fe serious discrepancies remain.

PACS number(s): 32.80.Wr, 23.40.−s

I. INTRODUCTION

Internal bremsstrahlung (IB) in electron capture is a process which has long been of interest. Since the pioneering theoretical studies by Möller [1] and Morrison and Schiff [2], many experimental investigations have been reported. Concomitantly, the theory of IB has undergone extensive development largely through the introduction of elaborate mathematical techniques by Glauber and Martin [3,4]. For allowed transitions agreement between theory and experiment is very good [5], and more recent investigations of IB have been concerned with the study of forbidden transitions and with the use of the IB process as a tool for measuring the mass of the electron neutrino.

Although less likely, double internal bremsstrahlung (DIB), i.e., the emission of two photons, may also occur in electron-capture decay. In this case both photons share the available energy statistically with the neutrino and thus have continuous energy distributions. The sum of the energies of the two photons also forms a continuous distribution, the end point of which yields the total energy released in the decay.

The probability with which DIB occurs is, of course, quite small. Because of the presence of an additional factor of α, the fine structure constant, and the reduction of the available phase space resulting from the presence of an additional photon, the probability for DIB is expected to be no greater than about 10^{-4} times the probability for IB. This alone makes observation of the phenomenon quite difficult and helps account for the fact that, over the years, little effort has been made to investigate it.

The first observations of the phenomenon were reported by Ljubičić, Jones, and Logan [6] (LJL), who investigated DIB in the electron-capture decay of ^{37}Ar. Using a dual parameter pulse-height analysis system, they observed the continous energy distribution of the two photons at an angle of 90° between the photon momenta and determined the distribution of the total energy of the photons over a substantial energy range.

Shortly thereafter, Pisk, Ljubičić, and Logan [7] provided the first theoretical study of the process based on the modern theory of the weak interactions. Following the approach of Morrison and Schiff [2], these authors performed a lowest-order perturbation theory calculation in which the effects of the nuclear Coulomb field on the intermediate electron states were neglected, these states being described by relativistic plane waves. For the initial electron states nonrelativistic Coulomb wave functions were used, with only contributions from zero-momentum states being taken into account. The actual calculations were limited to capture from the K shell.

The results of this theoretical work were found to give a reasonably good fit to the data of LJL for the sum-energy spectrum of ^{37}Ar. However, when an absolute comparison was made for the ratio of the DIB sum spectrum to the IB spectrum, the agreement was less than satisfactory.

These pioneering studies of the DIB process were followed by a series of papers by members of the original collaborations together with various co-workers in which they reported observations of DIB in ^{37}Ar at relative emission angles other than 90° [8], observations of DIB in ^{55}Fe [9,10] and in ^{131}Cs [11], and studies on the contributions to DIB at low energies from L- and M-shell electron capture [12,13]. The general pattern that emerged from this work was one of reasonable qualitative agreement between theory and experiment, but serious disagreement when quantitative comparisons were made.

In view of the important role that Coulomb effects are known to play in the IB process, it is clear that such effects must be taken fully into account in the theory of the DIB process before meaningful quantitative comparisons may be made. In this paper we shall develop the basic theory of the DIB process for allowed electron-capture transitions in an approximation in which the atomic electron is treated nonrelativistically but the effects of the nuclear Coulomb field are fully included. While this will restrict our results to nuclei whose nuclear charge is not too large, it will provide much more accurate results at lower energies where the spectra are most intense and

where the influence of the nuclear Coulomb field is greatest. Also, since most of the experimental data which have been reported thus far were taken at energies at which the process is completely dominated by electron capture from the K shell, we shall, in this paper, limit detailed calculations and numerical results to this case.

In Sec. II we develop the general formalism, establish the nonrelativistic approximations, and describe the calculation of the transition matrix element. In Sec. III the two-photon distribution function is obtained. Numerical results are presented in Sec. IV and compared with available experimental data. Section V contains our conclusions.

II. TRANSITION AMPLITUDE FOR DIB

A. General formalism

In the lowest order of perturbation theory, DIB is described by the two Feynman diagrams shown in Fig. 1. (By comparison, the contribution from diagrams involving nuclear intermediate states is negligible for allowed electron-capture transitions.) Adopting the usual $V-\lambda A$ theory for the weak interaction and employing standard methods [14], one readily obtains the following expression for the total probability amplitude associated with the two diagrams of Fig. 1:

$$S = 2\pi\delta(k_{\max} - k_1 - k_2 - E_\nu)M, \tag{1}$$

with the transition matrix element given by

$$\begin{aligned} M = Ge^2(1+P_{12}) \int d\vec{r}_n \int d\vec{r}_1 \int d\vec{r}_2 \phi_f(\vec{r}_n)\Gamma_\mu \phi_i(\vec{r}_n) \\ \times \bar{\phi}_\nu(\vec{r}_n)\Lambda_\mu G_{\epsilon'}(\vec{r}_n,\vec{r}_1)a_1^\dagger(\vec{r}_1) \\ \times G_\epsilon(\vec{r}_1,\vec{r}_2)a_2^\dagger(\vec{r}_2)\phi_e(\vec{r}_2), \end{aligned} \tag{2}$$

where $\Gamma_\mu = \gamma_\mu(1+\lambda\gamma_5)$, $\Lambda_\mu = \gamma_\mu(1+\gamma_5)$, and G is the vector coupling constant of the β interaction. Respectively, ϕ_i and ϕ_f represent the initial and final states of the nucleus, and ϕ_ν and ϕ_e (with associated energies E_ν and E_e) represent the states of the emitted neutrino and the initial electron. The energies of the two emitted photons are k_1 and k_2, and $k_{\max}$ is the energy released in the electron-capture process, to be shared statistically among the three emitted particles. The photon states are characterized by a_i defined by

$$a_i(\vec{r}) = \frac{1}{(2\pi)^{3/2}} \frac{\vec{\gamma}\cdot\hat{e}_i}{\sqrt{2k_i}} e^{i\vec{k}_i\cdot\vec{r}} \qquad (i=1,2), \tag{3}$$

where $\vec{k}_i$ and $\hat{e}_i$ are a photon's momentum and polarization vectors, respectively (satisfying $\vec{k}_i\cdot\hat{e}_i = 0$), and we have chosen $V=(2\pi)^3$ as the normalization volume. The operator P_{12} performs the interchanges ($\vec{k}_1 \leftrightarrow \vec{k}_2$, $\hat{e}_1 \leftrightarrow \hat{e}_2$) which connect the two Feynman diagrams in Fig. 1. Finally, the energies associated with each of the G_ϵ's, which describe the propagation of an electron moving in a nuclear Coulomb field, are given by $\epsilon = E_e - k_2$ and $\epsilon' = E_e - k_1 - k_2$.

For an allowed electron-capture transition the wave functions of the leptons involved in the β interaction can be replaced by their values at the origin. Furthermore, in the nonrelativistic limit the nuclear matrix elements, which we denote by B_μ, reduce to

$$(\phi_f\Gamma_\mu\phi_i) \rightarrow \{i\lambda(\phi_f,\vec{\sigma}\phi_i),(\phi_f,\phi_i)\} \equiv \left\{\vec{B}, B_4\right\}. \tag{4}$$

With the resulting simplifications the transition matrix element assumes the form [15]

$$M = \frac{\alpha G}{(2\pi)^2} \frac{(1+P_{12})}{\sqrt{k_1k_2}} \bar{\phi}_\nu(0)\mathcal{B}I_{12}, \tag{5}$$

with $\mathcal{B} = \Lambda_\mu B_\mu$ and $I_{12} \equiv I(\vec{k}_1,\hat{e}_1;\vec{k}_2,\hat{e}_2)$ with

$$\begin{aligned} I(\vec{k}_1,\hat{e}_1;\vec{k}_2,\hat{e}_2) = \int d\vec{r}_1 \int d\vec{r}_2 G_{\epsilon'}(0,\vec{r}_1)\vec{\gamma}\cdot\hat{e}_1 e^{-i\vec{k}_1\cdot\vec{r}_1} \\ \times G_\epsilon(\vec{r}_1,\vec{r}_2)\vec{\gamma}\cdot\vec{e}_2 e^{-i\vec{k}_2\cdot\vec{r}_2}\phi_e(\vec{r}_2). \end{aligned} \tag{6}$$

Each electron propagator G_E is represented by a Dirac-Coulomb Green's function which satisfies the pair of equations

$$[E - H(\vec{r})]\, G_E(\vec{r},\vec{r}')\gamma_4 = \delta(\vec{r}-\vec{r}'), \tag{7a}$$

and its adjoint

$$G_E(\vec{r},\vec{r}')\gamma_4[E - H(\vec{r}')] = \delta(\vec{r}-\vec{r}'), \tag{7b}$$

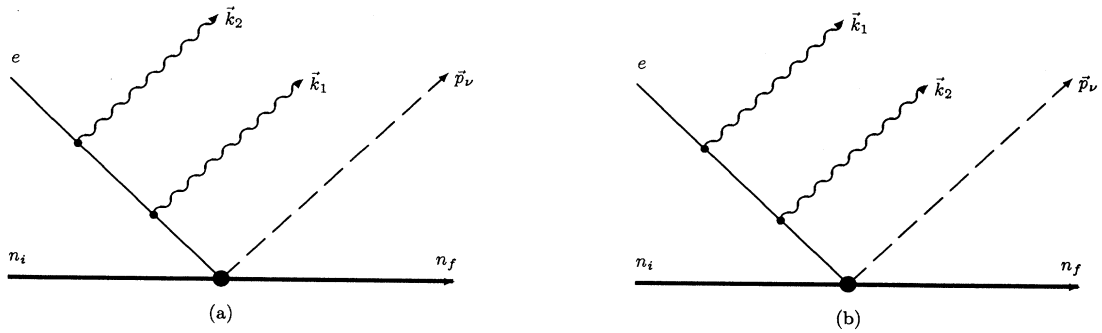

FIG. 1. Feynman diagrams for electron capture accompanied by double internal bremsstrahlung.

where H is the Dirac Hamiltonian for an electron moving in the nuclear Coulomb field. We shall only have need of the latter of these equations which, when written out explicitly for a point nucleus of charge Ze, becomes

$$G_E(\vec{r},\vec{r}')\left[\vec{\gamma}\cdot\overleftarrow{\nabla}' + 1 - \gamma_4(E + a/r')\right] = -\delta(\vec{r}-\vec{r}'), \quad (8)$$

where $a = Z\alpha$ and $\overleftarrow{\nabla}'$ acts on the function $G_E(\vec{r},\vec{r}')$ which precedes it as indicated by the direction of the arrow.

For purposes of calculation it is convenient to express the Dirac-Coulomb Green's function $G_E(\vec{r},\vec{r}')$ in terms of the Green's function $\mathcal{G}_E(\vec{r},\vec{r}')$ for the iterated or second-order form of the Dirac equation. Indeed, the effectiveness of this approach was first demonstrated by Glauber and Martin in their classic papers [3,4] on radiative electron capture; and, not surprisingly, it is equally useful in the study of DIB. Hence, following closely the work of these authors, we define the second-order Dirac-Coulomb Green's function so as to satisfy the equation

$$\mathcal{G}_E(\vec{r},\vec{r}')[\nabla'^2 + (E + a/r')^2 - 1 - i\vec{\alpha}\cdot\vec{\nabla}'(a/r')] = \delta(\vec{r}-\vec{r}'), \quad (9)$$

in which ∇'^2 acts to the left. The first-order Green's function may now be written in terms of the second-order Green's function as

$$G_E(\vec{r},\vec{r}') = \mathcal{G}_E(\vec{r},\vec{r}')[\vec{\gamma}\cdot\overleftarrow{\nabla}' + \gamma_4(E + a/r') + 1]. \quad (10)$$

Using this relationship we find that I_{12} may be written as

$$I_{12} = \int d\vec{r}_1 \int d\vec{r}_2\, \mathcal{G}_{\epsilon'}(0,\vec{r}_1)[\vec{\gamma}\cdot\overleftarrow{\nabla}_1 + \gamma_4(\epsilon' + a/r_1) + 1] \times e^{-i\vec{k}_1\cdot\vec{r}_1}\vec{\gamma}\cdot\hat{e}_1\mathcal{G}_\epsilon(\vec{r}_1,\vec{r}_2) \times[-i\vec{\gamma}\cdot\hat{e}_2\gamma_\mu k_{2\mu} - 2\hat{e}_2\cdot\vec{\nabla}_2]e^{-i\vec{k}_2\cdot\vec{r}_2}\phi_e(\vec{r}_2), \quad (11)$$

after an integration by parts has been performed with respect to $\vec{r}_2$ and use has been made of the fact that the wave function of the initial electron ϕ_e satisfies $H\phi_e = E_e\phi_e$.

In the next section we shall describe in detail the representations to be used for the second-order Green's functions. For now, in order to complete our formulation of the problem in general terms, we simply wish to anticipate that it will be convenient to describe the "outer" Green's function $\mathcal{G}_\epsilon(\vec{r}_1,\vec{r}_2)$, as well as the wave function of the initial electron ϕ_e, by means of the Fourier integral representations

$$\mathcal{G}_\epsilon(\vec{r}_1,\vec{r}_2) = \frac{1}{(2\pi)^3}\int d\vec{p}_1 \int d\vec{p}_2\, \tilde{\mathcal{G}}_\epsilon(\vec{p}_1,\vec{p}_2)e^{i(\vec{p}_1\cdot\vec{r}_1 - \vec{p}_2\cdot\vec{r}_2)} \quad (12)$$

and

$$\phi_e(\vec{r}) = \frac{1}{(2\pi)^{3/2}}\int d\vec{p}\tilde{\phi}_e(\vec{p})e^{i\vec{p}\cdot\vec{r}}, \quad (13)$$

which serve to define $\tilde{\mathcal{G}}_\epsilon(\vec{p}_1,\vec{p}_2)$ and $\tilde{\phi}_e(\vec{p})$. With the introduction of these forms, an integration by parts with respect to $\vec{r}_1$ may be performed after which the integration over $\vec{r}_2$, followed by the integration over $\vec{p}$, may be carried out by elementary methods. The result of all this integration is the following expression for I_{12}:

$$I_{12} = \frac{1}{(2\pi)^{3/2}}\int d\vec{p}_1 \int d\vec{p}_2 \int d\vec{r}_1\, \mathcal{G}_{\epsilon'}(0,\vec{r}_1)e^{i\vec{q}_1\cdot\vec{r}_1}\,[-i\vec{\gamma}\cdot\vec{q}_1 + \gamma_4(\epsilon' + a/r_1) + 1]\,\vec{\gamma}\cdot\hat{e}_1\tilde{\mathcal{G}}_\epsilon(\vec{p}_1,\vec{p}_2) \times[-i\vec{\gamma}\cdot\hat{e}_2\gamma_\mu k_{2\mu} - 2i\hat{e}_2\cdot\vec{q}_2]\,\tilde{\phi}_e(\vec{q}_2), \quad (14)$$

where $\vec{q}_1 = \vec{p}_1 - \vec{k}_1$ and $\vec{q}_2 = \vec{p}_2 + \vec{k}_1$. To proceed further with our analysis, it is necessary to choose specific forms for the Green's functions and the wave function of the initial electron.

B. Nonrelativistic approximations

For moderately light nuclei the initial electronic state can be adequately represented by a nonrelativistic Coulomb wave function; and in view of the far greater complexity attendant on the use of Dirac-Coulomb wave functions, it is important to consider first the nonrelativistic regime. In general, this is expected to yield results with a relative accuracy of order $Z\alpha$.

A particular advantage of introducing the second-order Green's function is that, consistent with the use of a nonrelativistic wave function for the initial electron, one can employ an approximate Green's function which has a much simpler structure. This approximate Green's function is obtained by neglecting the fine structure terms $(a/r')^2$ and $\vec{\alpha}\cdot\vec{\nabla}'(a/r')$ in Eq. (9). The second-order Green's function may then by written in the form $\mathcal{G}_E(\vec{r},\vec{r}') = I\mathcal{G}'_E(\vec{r},\vec{r}')$ where I is a unit matrix and $\mathcal{G}'_E(\vec{r},\vec{r}')$ is a scalar Green's function which satisfies the equation

$$\mathcal{G}'_E(\vec{r},\vec{r}')\left[\nabla'^2 + E^2 - 1 + 2aE/r'\right] = \delta(\vec{r}-\vec{r}'). \quad (15)$$

This equation has the same form as that satisfied by the nonrelativistic Coulomb Green's function and is readily reduced to the latter equation by defining $\bar{a} = aE$, $\mathcal{E} = (E^2-1)/2$, and $G_\mathcal{E}(\vec{r},\vec{r}') = 2\mathcal{G}'_E(\vec{r},\vec{r}')$. Then $G_\mathcal{E}(\vec{r},\vec{r}')$ satisfies

$$[\mathcal{E} - H_{\rm nr}(\vec{r}')]\,G_\mathcal{E}(\vec{r},\vec{r}') = \delta(\vec{r}-\vec{r}'), \quad (16)$$

where $H_{\rm nr}(\vec{r}') = -\nabla'^2/2 - \bar{a}/r'$.

The particular function $\mathcal{G}'_{\epsilon'}(0,r_1)$ which will be used to

represent the "inner" Green's function has been studied in considerable detail by Glauber and Martin [3]. In particular, these authors have shown that $\mathcal{G}'_{\epsilon'}(0,r)$ possesses the following integral representation [16]:

$$\mathcal{G}'_{\epsilon'}(0,r) = -\frac{\mu}{2\pi} e^{-\mu r} \int_0^\infty ds \left(\frac{1+s}{s}\right)^\eta e^{-2\mu r s}, \quad (17)$$

where $\mu = (1-\epsilon'^2)^{1/2}$ and $\eta = a\epsilon'/\mu$.

With regard to the "outer" Green's function the situation is more complicated, and we approach its construction by first transforming to momentum space via the Fourier transforms introduced earlier. In view of the simple connection between the approximate second-order Green's function and the nonrelativistic Coulomb Green's function discussed above, it follows that, within the approximation that we have adopted, we may write $\tilde{\mathcal{G}}'_\epsilon(\vec{p}_1,\vec{p}_2) = \frac{1}{2}\tilde{G}_\mathcal{E}(\vec{p}_1,\vec{p}_2)$ where $\tilde{G}_\mathcal{E}(\vec{p}_1,\vec{p}_2)$ is the nonrelativistic Coulomb Green's function in momentum space. For this latter Green's function three equivalent representations due to Schwinger [18] are available, the most suitable form for our purposes being that given by Eq. (1′) of Schwinger's paper, viz.,

$$\tilde{G}_\mathcal{E}(\vec{p}_1,\vec{p}_2) = \tilde{G}^{(0)}_\mathcal{E}(\vec{p}_1,\vec{p}_2) + \tilde{G}^{(1)}_\mathcal{E}(\vec{p}_1,\vec{p}_2) + \tilde{G}^{(2)}_\mathcal{E}(\vec{p}_1,\vec{p}_2), \quad (18)$$

with the three contributions to $\tilde{G}_\mathcal{E}(\vec{p}_1,\vec{p}_2)$ defined by

$$\tilde{G}^{(0)}_\mathcal{E}(\vec{p}_1,\vec{p}_2) = \frac{\delta(\vec{p}_1-\vec{p}_2)}{(\mathcal{E}-p_1^2/2)}, \quad (19)$$

$$\tilde{G}^{(1)}_\mathcal{E}(\vec{p}_1,\vec{p}_2) = -\frac{\bar{a}}{2\pi^2}\frac{1}{(\mathcal{E}-p_1^2/2)}\frac{1}{(\vec{p}_1-\vec{p}_2)^2}\frac{1}{(\mathcal{E}-p_2^2/2)}, \quad (20)$$

$$\tilde{G}^{(2)}_\mathcal{E}(\vec{p}_1,\vec{p}_2) = -\frac{\bar{a}}{2\pi^2}\frac{1}{(\mathcal{E}-p_1^2/2)}\frac{1}{(\mathcal{E}-p_2^2/2)}\nu\int_0^1 d\rho\left[\frac{\rho^{-\nu}}{\{(\vec{p}_1-\vec{p}_2)^2\rho-(\mathcal{E}-p_1^2/2)(\mathcal{E}-p_2^2/2)(1-\rho)^2/2\mathcal{E}\}}\right], \quad (21)$$

where now $\bar{a} = a\epsilon$ and $\mathcal{E} = (\epsilon^2-1)/2$, and ν is defined by $\nu = \bar{a}/\sqrt{-2\mathcal{E}}$.

As the notation suggests, $\tilde{G}^{(0)}_\mathcal{E}(\vec{p}_1,\vec{p}_2)$ corresponds to a free-particle approximation while the other two contributions take into account Coulomb effects. Thus, by employing this particular representation for the "outer" Green's function, one can readily investigate the influence of Coulomb effects on the "inner" Green's function alone by approximating the "outer" Green's function by $\tilde{G}^{(0)}_\mathcal{E}(\vec{p}_1,\vec{p}_2)$. In addition, this representation possesses the practical advantage of permitting the most efficient computation of numerical results since it lends itself to the highest degree of parallelization, and the numerical methods that must be invoked show superior numerical stability.

The relative importance of the two Coulomb terms may be judged by examining the dependence on the photon energy k_2 of the quantity ν which appears in the definition of $\tilde{G}^{(2)}_\mathcal{E}(\vec{p}_1,\vec{p}_2)$. As is readily confirmed, ν assumes it largest value at $k_2 = 0$ where it is slightly less than one. (It differs from unity by terms of order a^2.) As k_2 increases, ν rapidly decreases, declining to values of order a or smaller as soon as k_2 is beyond the binding-energy region, i.e., $\nu \leq a$ for $k_2 \gg a^2/2$. Therefore, for photon energies above the binding-energy region, it becomes consistent with our previous approximations to employ for the "outer" Green's function the approximation

$$\tilde{G}_\mathcal{E}(\vec{p}_1,\vec{p}_2) \approx \tilde{G}^{(0)}_\mathcal{E}(\vec{p}_1,\vec{p}_2) + \tilde{G}^{(1)}_\mathcal{E}(\vec{p}_1,\vec{p}_2). \quad (22)$$

In view of the fact that this approximation is well satisfied by essentially all currently available experimental data, it will be adopted in this paper as the basis for detailed calculations and the computation of numerical results.

Finally, we must choose the state of the initial electron so that the form of its wave function may be specified. As previously discussed, in this paper detailed calculations will be limited to radiative capture from the K shell for which the Fourier transform of the nonrelativistic Coulomb form for $\phi_K(r)$ is readily found to be

$$\tilde{\phi}_K(p) = \frac{(2a)^{3/2}}{\pi}\frac{a}{(a^2+p^2)^2}\chi_K, \quad (23)$$

where χ_K determines the spin state of the initial K electron. Equipped with the above representations, we are ready to proceed with the evaluation of Eq. (14).

C. Evaluation

We begin the evaluation of I_{12} by introducing the Glauber-Martin representation Eq. (17), along with Eq. (23), into Eq. (14) and performing the integration over $\vec{r}_1$. This yields the result

$$I_{12} = \mu\left(\frac{a}{\pi}\right)^{5/2}\int_0^\infty ds\left(\frac{1+s}{s}\right)^\eta \int d\vec{p}_1 \int d\vec{p}_2 \frac{1}{(a^2+q_2^2)^2}\left[\{-i\vec{\gamma}\cdot\vec{q}_1+\gamma_4\epsilon'+1\}\frac{2\sigma}{(\sigma^2+q_1^2)^2}+a\gamma_4\frac{1}{(\sigma^2+q_1^2)}\right]$$
$$\times\tilde{G}_\mathcal{E}(\vec{p}_1,\vec{p}_2)\vec{\gamma}\cdot\hat{e}_1\left[\vec{\gamma}\cdot\hat{e}_2\gamma_\mu k_{2\mu}+2i\hat{e}_2\cdot\vec{q}_2\right]\chi_K, \quad (24)$$

where $\sigma = \mu(2s+1)$. To organize our further calculations, it is convenient at this point to introduce a set of functions of $\vec{k}_1$ and $\vec{k}_2$ which, for the sake of discussion, we shall henceforth refer to as amplitude functions. The set of functions and its members are denoted by $\Lambda = \{S_0, S_1, \vec{V}_0, \vec{V}_1, \vec{V}_2, T_{ij}\}$ and, by definition, satisfy the set of equations

$$\Lambda = \int_0^\infty ds \left(\frac{1+s}{s}\right)^\eta \int d\vec{p}_1 \int d\vec{p}_2 \frac{\tilde{G}_\varepsilon(\vec{p}_1,\vec{p}_2)}{(a^2+q_2^2)^2}\Sigma, \quad (25)$$

where Σ is defined as the set $\Sigma = \{s_0, s_1, \vec{v}_0, \vec{v}_1, \vec{v}_2, t_{ij}\}$ whose members are defined by

$$s_0 = 1/(\sigma^2+q_1^2), \quad (26a)$$
$$s_1 = 2\sigma/(\sigma^2+q_1^2)^2, \quad (26b)$$
$$\vec{v}_0 = \vec{q}_2/(\sigma^2+q_1^2), \quad (26c)$$
$$\vec{v}_1 = 2\sigma\vec{q}_1/(\sigma^2+q_1^2)^2, \quad (26d)$$
$$\vec{v}_2 = 2\sigma\vec{q}_2/(\sigma^2+q_1^2)^2, \quad (26e)$$
$$t_{ij} = 2\sigma q_{1i}q_{2j}/(\sigma^2+q_1^2)^2. \quad (26f)$$

In terms of these amplitude functions I_{12} may be written as

$$I_{12} = \mu\left(\frac{a}{\pi}\right)^{5/2} A_{12}\chi_K, \quad (27)$$

with $A_{12} \equiv A(\vec{k}_1, \hat{e}_1; \vec{k}_2, \hat{e}_2)$ and

$$\begin{aligned} A(\vec{k}_1,\hat{e}_1;\vec{k}_2,\hat{e}_2) = &\left[-i\vec{\gamma}\cdot\vec{V}_1 + (\gamma_4\epsilon'+1)\,S_1 + a\gamma_4 S_0\right] \\ &\times\vec{\gamma}\cdot\hat{e}_1\vec{\gamma}\cdot\hat{e}_2\gamma_\mu k_{2\mu} \\ &+2i[-i\gamma_i T_{ij}e_{2j} + (\gamma_4\epsilon'+1)\,\hat{e}_2\cdot\vec{V}_2 \\ &+a\gamma_4\hat{e}_2\cdot\vec{V}_0]\vec{\gamma}\cdot\hat{e}_1. \end{aligned} \quad (28)$$

The amplitude functions lend themselves to considerable analytic reduction after which numerical methods must be used to complete their evaluation. The details of this analytical work along with final formulas suitable for numerical integration are contained in Appendix A. To conclude this section, we combine Eqs. (5) and (27) to obtain the following final expression for the DIB transition matrix element:

$$M = \frac{\alpha G}{(2\pi)^2}\left(\frac{a}{\pi}\right)^{5/2}\frac{\mu}{\sqrt{k_1k_2}}\bar{\phi}_\nu(0)\mathcal{B}\,(A_{12}+A_{21})\,\chi_K, \quad (29)$$

where A_{12} is given by Eq. (28).

III. TWO-PHOTON DISTRIBUTION FUNCTION

The transition rate $dw_{\gamma\gamma}$ for the emission of two photons with momenta in the ranges $d\vec{k}_1$ and $d\vec{k}_2$ during an allowed K-capture transition is related to M by Fermi's golden rule, i.e.,

$$dw_{\gamma\gamma} = 2\pi \mid M \mid^2 \delta(k_{\max} - k_1 - k_2 - E_\nu)d\vec{k}_1 d\vec{k}_2 d\vec{p}_\nu, \quad (30)$$

where $\vec{p}_\nu$ is the momentum of the emitted neutrino.

Since the neutrino is unobserved and two K electrons are normally present initially, we must integrate the differential transition rate over the neutrino's momentum and sum it over the spin states of the neutrino and the initial electron. With the introduction of Eqs. (29) and (28) into Eq. (30) and the use of standard projection operator techniques to perform the spin sums, these operations lead to the following result for the differential transition rate for the emission of two photons with energies and directions within dk_1, dk_2 and $d\Omega_1$,$d\Omega_2$ of $\vec{k}_1$,$\vec{k}_2$, respectively [17]:

$$\begin{aligned} dw_{\gamma\gamma} = W_K\frac{(2\alpha a\mu)^2}{(2\pi)^8}k_1k_2\left[1-(k_1+k_2)/k_{\max}\right]^2 \\ \times\sum_{\text{pol}}\text{Tr}\Big[(1+\gamma_4)(A_{12}^\dagger + A_{21}^\dagger) \\ \times(1+\gamma_5)(A_{12}+A_{21})\Big]dk_1dk_2d\Omega_1d\Omega_2, \end{aligned} \quad (31)$$

where, assuming that the polarizations of the photons are unobserved, $\sum_{\text{pol}}$ indicates a summation over the polarization states of the two photons, and W_K is the transition rate for nonradiative K capture which is given by Eq. (B1) of Appendix B.

The tasks of performing the indicated polarization sum and evaluating the trace appearing in Eq. (31) remain. These calculations, performed using standard techniques, are straightforward but exceedingly tedious. We present only the final results, most easily stated by first defining

$$T_a(\vec{k}_1,\vec{k}_2) = \sum_{\text{pol}}\text{Tr}\left[(1+\gamma_4)A_{12}^\dagger(1+\gamma_5)A_{12}\right], \quad (32a)$$

$$T_b(\vec{k}_1,\vec{k}_2) = \sum_{\text{pol}}\text{Tr}\left[(1+\gamma_4)A_{12}^\dagger(1+\gamma_5)A_{21}\right], \quad (32b)$$

with which the DIB transition rate may then by written as

$$\begin{aligned} dw_{\gamma\gamma} = W_K\frac{(2\alpha a\mu)^2}{(2\pi)^8}k_1k_2\left[1-(k_1+k_2)/k_{\max}\right]^2 \\ \times\left[T_a(\vec{k}_1,\vec{k}_2)+T_a(\vec{k}_2,\vec{k}_1)+2\text{Re}\{T_b(\vec{k}_1,\vec{k}_2)\}\right] \\ \times dk_1dk_2d\Omega_1d\Omega_2, \end{aligned} \quad (33)$$

where Re denotes the real part of the accompanying function. To express our final results for T_a and T_b as compactly as possible, we first define

$$S_2 = aS_0 + \epsilon' S_1, \quad (34)$$
$$\vec{V}_3 = a\vec{V}_0 + \epsilon'\vec{V}_2, \quad (35)$$

and, to distinguish between direct and exchange terms, we also introduce

$$P_n \equiv P_n(\vec{k}_1,\vec{k}_2) = S_n(\vec{k}_2,\vec{k}_1) \quad (n=1,2), \quad (36)$$
$$\vec{A}_n \equiv \vec{A}_n(\vec{k}_1,\vec{k}_2) = \vec{V}_n(\vec{k}_2,\vec{k}_1) \quad (n=1,3), \quad (37)$$
$$G_{ij} \equiv G_{ij}(\vec{k}_1,\vec{k}_2) = T_{ij}(\vec{k}_2,\vec{k}_1) \quad (i,j=1,3). \quad (38)$$

In terms of these quantities T_a is found to be given by

$$T_a(\vec{k}_1,\vec{k}_2) = 32\Big[k_2^2\left(\vec{V}_1\cdot\vec{V}_1+S_1^2+S_2^2\right)-2\mu_{12}k_2^2S_2\vec{V}_1\cdot\hat{n}_1+k_2\hat{n}_1\times\vec{V}_1\cdot T\cdot\vec{n}_1-\mu_{12}k_2\hat{n}_1\times\vec{V}_1\cdot T\cdot\vec{n}_2$$
$$+k_2\left(S_1-S_2\right)\hat{n}_1\cdot T\cdot\hat{n}_1\times\hat{n}_2-k_2\vec{V}_1\cdot\hat{n}_1\left(\vec{V}_3-\vec{V}_2\right)\cdot\hat{n}_1\times\hat{n}_2+T_{ij}T_{ij}-T_{ij}n_{2j}T_{ik}n_{2k}$$
$$+\left(\vec{V}_3-\vec{V}_2\right)^2-\left\{\left(\vec{V}_3-\vec{V}_2\right)\cdot\hat{n}_2\right\}^2\Big], \tag{39}$$

where $\hat{n}_i = \vec{k}_i/k_i, (i = 1,2)$, $\mu_{12} = \hat{n}_1\cdot\hat{n}_2$, e_{ijk} is the permutation symbol (used below), and the summation convention is invoked with respect to the Cartesian indices i,j,k which appear. The final expression for T_b proves to be considerably more complicated, leading us to write it as a sum of terms

$$T_b(\vec{k}_1,\vec{k}_2) = 16\left(T_{b1}+T_{b2}+T_{b3}+T_{b4}+T_{b5}+T_{b6}+T_{b7}\right), \tag{40}$$

with the individual contributions to T_b found to be given by

$$T_{b1} = \frac{k_1k_2}{2}\Big[\left(\vec{V}_1\cdot\vec{A}_1+S_1P_1+S_2P_2\right)\left(\mu_{12}^2-1\right)+\left(P_2\vec{V}_1+S_2\vec{A}_1\right)\cdot\left(\hat{n}_1+\hat{n}_2\right)\left(\mu_{12}-1\right)-\vec{V}_1\times\vec{A}_1\cdot\hat{n}_1\times\hat{n}_2$$
$$+\vec{V}_1\cdot\hat{n}_1\vec{A}_1\cdot\hat{n}_2\mu_{12}-\vec{V}_1\cdot\hat{n}_2\vec{A}_1\cdot\hat{n}_1\mu_{12}+S_1\left\{\vec{A}_1\cdot\left(\hat{n}_2-\hat{n}_1\right)\left(\mu_{12}+1\right)+P_2\left(\mu_{12}^2-1\right)\right\}$$
$$+P_1\left\{-\vec{V}_1\cdot\left(\hat{n}_2-\hat{n}_1\right)\left(\mu_{12}+1\right)+S_2\left(\mu_{12}^2-1\right)\right\}\Big], \tag{41a}$$

$$T_{b2} = -k_2S_1\left[n_{2k}e_{kij}G_{ij}-\hat{n}_1\times\hat{n}_2\cdot G\cdot\hat{n}_1\right]-k_1P_1\left[n_{1k}e_{kij}T_{ij}+\hat{n}_1\times\hat{n}_2\cdot T\cdot\hat{n}_2\right], \tag{41b}$$

$$T_{b3} = \Big[\vec{A}_2\cdot\vec{V}_2-\vec{A}_2\cdot\hat{n}_1\vec{V}_2\cdot\hat{n}_1-\vec{A}_2\cdot\hat{n}_2\vec{V}_2\cdot\hat{n}_2+\mu_{12}\vec{A}_2\cdot\hat{n}_1\vec{V}_2\cdot\hat{n}_2-\vec{V}_2\cdot\vec{A}_3+\vec{V}_2\cdot\hat{n}_1\vec{A}_3\cdot\hat{n}_1$$
$$+\vec{V}_2\cdot\hat{n}_2\vec{A}_3\cdot\hat{n}_2-\mu_{12}\vec{V}_2\cdot\hat{n}_2\vec{A}_3\cdot\hat{n}_1-\vec{V}_3\cdot\vec{A}_2+\vec{V}_3\cdot\hat{n}_2\vec{A}_2\cdot\hat{n}_2+\vec{V}_3\cdot\hat{n}_1\vec{A}_2\cdot\hat{n}_1-\mu_{12}\vec{V}_3\cdot\hat{n}_2\vec{A}_2\cdot\hat{n}_1\Big], \tag{41c}$$

$$T_{b4} = k_1\Big[\vec{V}_2\times\vec{A}_1\cdot\hat{n}_1-\vec{V}_2\cdot\hat{n}_2\vec{A}_1\cdot\hat{n}_1\times\hat{n}_2-A_{1k}e_{kij}T_{ij}-\vec{A}_1\times\hat{n}_2\cdot T\cdot\hat{n}_2-\vec{V}_3\times\vec{A}_1\cdot\hat{n}_1$$
$$+\vec{V}_3\cdot\hat{n}_2\vec{A}_1\cdot\hat{n}_1\times\hat{n}_2+P_2n_{1k}e_{kij}T_{ij}+P_2\hat{n}_1\times\hat{n}_2\cdot T\cdot\hat{n}_2\Big], \tag{41d}$$

$$T_{b5} = k_2\Big[\vec{V}_1\times\vec{A}_3\cdot\hat{n}_2-\vec{A}_3\cdot\hat{n}_1\vec{V}_1\cdot\hat{n}_1\times\hat{n}_2-V_{1k}e_{kij}G_{ij}-\vec{V}_1\times\hat{n}_1\cdot G\cdot\hat{n}_1-\vec{V}_1\times\vec{A}_2\cdot\hat{n}_2$$
$$+\vec{A}_2\cdot\hat{n}_1\vec{V}_1\cdot\hat{n}_1\times\hat{n}_2+S_2n_{2k}e_{kij}G_{ij}-S_2\hat{n}_1\times\hat{n}_2\cdot G\cdot\hat{n}_1\Big], \tag{41e}$$

$$T_{b6} = \Big[T_{ij}G_{ij}-T_{ij}G_{ik}\left(n_{1j}n_{1k}+n_{2j}n_{2k}-\mu_{12}n_{2j}n_{1k}\right)+\vec{V}_3\cdot\vec{A}_3-\vec{V}_3\cdot\hat{n}_1\vec{A}_3\cdot\hat{n}_1-\vec{V}_3\cdot\hat{n}_2\vec{A}_3\cdot\hat{n}_2$$
$$+\mu_{12}\vec{V}_3\cdot\hat{n}_2\vec{A}_3\cdot\hat{n}_1\Big], \tag{41f}$$

$$T_{b7} = [T_{ij}G_{ji}-\hat{n}_1\cdot T\cdot G\cdot\hat{n}_1-\hat{n}_2\cdot G\cdot T\cdot\hat{n}_2+\hat{n}_1\cdot T\cdot\hat{n}_2\,\hat{n}_2\cdot G\cdot\hat{n}_1-G_{ii}T_{jj}+\hat{n}_1\cdot G\cdot\hat{n}_1T_{ii}$$
$$+\hat{n}_2\cdot T\cdot\hat{n}_2G_{ii}-\hat{n}_1\cdot G\cdot\hat{n}_1\,\hat{n}_2\cdot T\cdot\hat{n}_2]. \tag{41g}$$

IV. RESULTS AND COMPARISON WITH EXPERIMENTS

To obtain numerical results, one must first evaluate the zero- and first-order amplitude functions, starting with Eqs. (A7) and (A16) and associated equations. The several multidimensional integrations are most efficiently performed by using the technique of Monte Carlo integration for which we employ the very powerful adaptive Monte Carlo subroutine VEGAS due to Lepage [19]. Using a Silicon Graphics IRIS Indigo R4400 workstation, we have found it feasible to configure VEGAS to yield results for our amplitude functions having a one standard deviation error estimate of not more than 1%, and all results presented in this paper have a *computational* error of this order.

We consider first the two-photon distribution function. As we shall discuss in more detail below, very few experimental data on the DIB process are presently available, and most that are were taken at an angle of 90° between the momentum vectors of the two photons. Therefore in this paper we shall limit our computational efforts to the evaluation of the energy distribution of the two photons for a relative emission angle of 90° only.

For tabulation purposes we normalize our results for the two-photon transition rate, as given by Eq. (33), to the transition rate for ordinary (nonradiative) K capture. Representative results for ^{37}Ar and ^{55}Fe are displayed in Tables I and II, respectively. When a comparison is made with the theory of Pisk *et al.* [7], it is found that the two theories yield predictions for the two-photon distribution function which are similar in form, but that the inclu-

TABLE I. Theoretical energy distribution of photons emitted in DIB at a relative angle of 90° for ^{37}Ar. The values shown are of the ratio $(dw_{\gamma\gamma}/dk_1dk_2d\Omega_1d\Omega_2)/W_K \times 10^{11}$ in units of $(mc^2)^{-2}(sr)^{-2}$.

k_2/k_{max}									
	0.8	6.34							
	0.7	24.3	12.5						
	0.6	53.1	46.4	17.9					
	0.5	93.6	96.3	61.6	20.3				
	0.4	149	163	121	98.4	20.3			
	0.3	231	241	244	121	61.6	17.9		
	0.2	351	372	241	163	96.3	46.4	12.5	
	0.1	498	351	231	149	93.6	53.1	24.3	6.34
		0.1	0.2	0.3	0.4	0.5	0.6	0.7	0.8
					k_1/k_{max}				

sion of Coulomb effects produces an overall reduction in intensity of roughly 20% [20].

The only published experimental data on the two-photon energy distribution are those of Ljubičić, Jones, and Logan [6] for ^{37}Ar. But the experimental data have been reported directly as counting rates versus the energies of the two photons and thus deviate substantially from the actual intensity distribution due to the resolution and sensitivity of the detectors used. Since the necessary corrections are not known, a direct comparison of these data with the present theory is not possible.

Because the counting rate in DIB experiments is very low, it is extremely difficult to get good statistics for the two-photon energy distribution. This has led experimenters to sum their data over the energy range of their experiment (with the sum of the energies of the two photons kept constant) and present their data in the form of a sum-energy spectrum. Such spectra were reported in Ref. [6] for ^{37}Ar and in Ref. [9] for ^{55}Fe. But, once again, these spectra were reported directly as counting rates and require correction for the efficiencies of the detectors before they can be compared with theory. Since these corrections are not known, we have been forced to use a less direct method of comparison.

Considering the ^{37}Ar case as being representative, first we compare the theoretical sum-energy spectrum predicted by the present theory with that predicted by the theory of Pisk *et al.* for the experimental conditions under which the ^{37}Ar data were obtained. Specifically, we calculate the two theoretical sum-energy spectra for the sum-energy range 210–810 keV using Eq. (42) shown below with a minimum detectable photon energy of $E_0 = 105$ keV and a detector bin width of $\Delta E = 50$ keV. Plots of the resulting sum-energy spectra are shown in Fig. 2. They reflect the similarity of form for the two-photon distribution function that was noted above. Indeed, the two curves shown have almost identical shapes and almost completely overlap when they are scaled to a common maximum. The principal difference between them is the overall reduction of intensity which is brought about by the inclusion of Coulomb effects.

Because of this similarity of shape, we may anticipate that, if the sum-energy spectrum predicted by the present theory were adjusted for detector efficiency and normalization and then plotted, the resulting curve would look very similar to that obtained from the theory of Pisk *et al.*, and agreement with the experimental data would probably be just about as good as that shown in Fig. 3 of Pisk *et al.* From this we conclude that the shape of the sum-energy spectrum is not very sensitive to Coulomb effects and that only an absolute determination of the sum-energy spectrum will reveal the predicted reduction of intensity due to the influence of the nuclear Coulomb field.

At present the only experimental data which do permit an absolute comparison between theory and experiment are those for $W_{DIB}(E, 90°)/W_{IB}(E)$, the ratio of the DIB sum-energy probability distribution to the probability distribution for the emission of a single IB photon. Such data have been reported in Ref. [6] for ^{37}Ar and in

TABLE II. Theoretical energy distribution of photons emitted in DIB at a relative angle of 90° for ^{55}Fe. The values shown are of the ratio $(dw_{\gamma\gamma}/dk_1dk_2d\Omega_1d\Omega_2)/W_K \times 10^{11}$ in units of $(mc^2)^{-2}(sr)^{-2}$.

k_2/k_{max}									
	0.8	2.36							
	0.7	10.2	4.37						
	0.6	25.2	19.4	6.04					
	0.5	50.4	45.7	24.8	6.75				
	0.4	86.8	85.6	57.0	27.9	6.75			
	0.3	143	142	103	57.0	24.8	6.04		
	0.2	215	203	142	85.6	45.7	19.4	4.37	
	0.1	265	215	143	86.8	50.4	25.2	10.2	2.36
		0.1	0.2	0.3	0.4	0.5	0.6	0.7	0.8
					k_1/k_{max}				

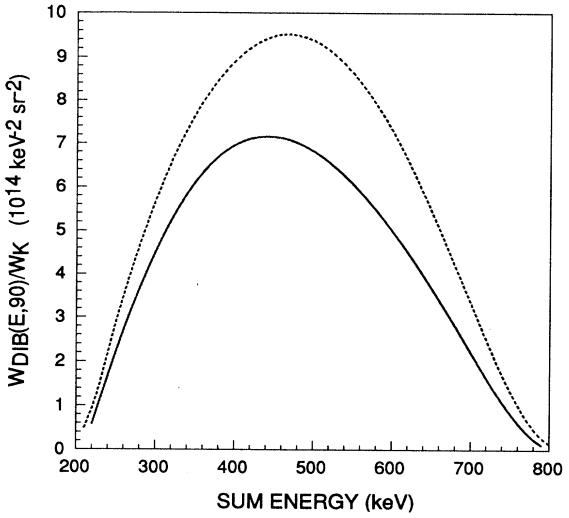

FIG. 2. The ^{37}Ar sum-energy spectrum for the experimental conditions of Ljubičić, Jones, and Logan. The dashed curve represents the prediction of the theory of Pisk *et al.* while the solid curve is the prediction of the present theory.

Ref. [9] for ^{55}Fe and can be compared with the theoretical predictions by employing the relations [21]

$$\int_{E-\Delta E/2}^{E+\Delta E/2} dk \int_0^{k-2E_0} dk_- \frac{dw_{\gamma\gamma}(\theta=90°)}{dk_1 dk_2 d\Omega_1 d\Omega_2}$$

$$= \frac{\Delta E^2}{2} W_{\mathrm{DIB}}(E,90°), \quad (42)$$

$$\int_{E-\Delta E/2}^{E+\Delta E/2} dk \frac{dw_\gamma}{dk d\Omega} = \Delta E\, W_{\mathrm{IB}}(E), \quad (43)$$

where $k = k_1 + k_2$, $k_- = k_1 - k_2$, and E is the measured DIB sum energy, ΔE is the energy width of the detector bins, and E_0 is the minimum detectable photon energy. For the present theory $dw_{\gamma\gamma}$ is given by Eq. (33) while, to comparable accuracy, dw_γ is given by the well-known result of Glauber and Martin [3] which we have reproduced in Appendix B. For the theory of Pisk *et al.* $dw_{\gamma\gamma}$ is given by Eq. (8) of their paper and, to the same level of accuracy as was used in Pisk's calculation, dw_γ is given by the familiar result of Morrison and Schiff [2], reproduced by Pisk *et al.* as their Eq. (A4). The employment of these theoretical expressions in Eqs. (42) and (43) above produces the results shown in Figs. 3 and 4 for ^{37}Ar and ^{55}Fe, respectively. For comparison we have also reproduced in these figures the experimental data of Refs. [6,9].

In the case of ^{37}Ar the results of the present theory appear to improve agreement with the experimental data. However, the fact that the two theories differ most at high energies makes one suspect that their differences are more likely to be due to the omission of relativistic effects in the present theory. (Pisk *et al.* use relativistic plane waves to describe the intermediate electron states.)

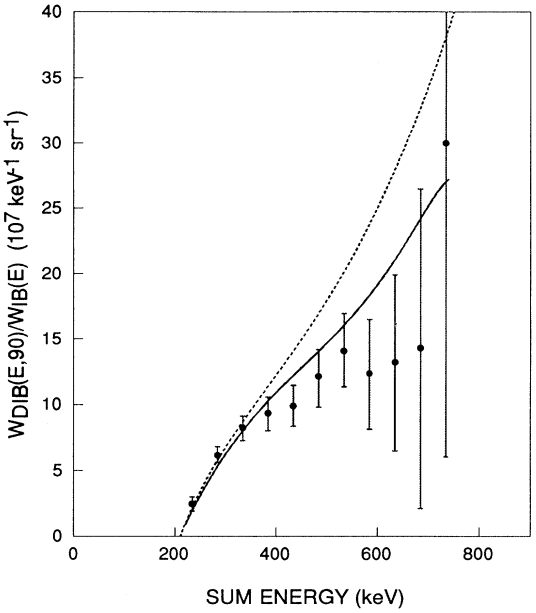

FIG. 3. The ratio $W_{\mathrm{DIB}}(E,90°)/W_{\mathrm{IB}}(E)$ as a function of the photon sum energy E for ^{37}Ar. The experimental results are from Ljubičić, Jones, and Logan and the two curves shown represent the predictions of Pisk *et al.* (dashed curve) and the present work (solid curve).

However, it can also be argued that the cumulative effect of neglecting the influence of the nuclear Coulomb field will be greater at high sum energies. Whatever the cause, we observe that in the case of ^{55}Fe, for which the spectrum end point occurs at a much lower energy, there is little difference between the predictions of the two theories and thus no resolution of the disagreement with the experimental data.

However, it is important to recognize that the ratio $W_{\mathrm{DIB}}(E,90°)/W_{\mathrm{IB}}(E)$ does not provide a sensitive test for Coulomb effects in the DIB process since, as has been pointed out by Pisk *et al.*, effects due to the in-

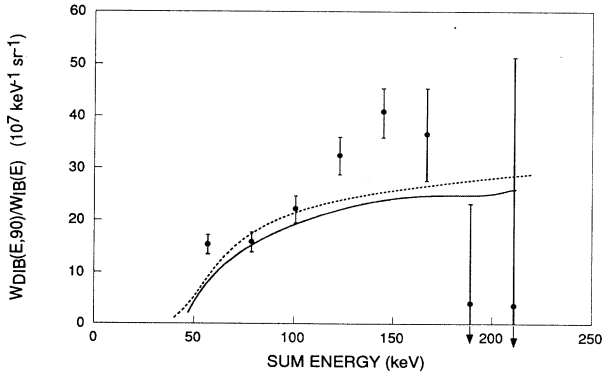

FIG. 4. The ratio $W_{\mathrm{DIB}}(E,90°)/W_{\mathrm{IB}}(E)$ as a function of the photon sum energy E for ^{55}Fe. The experimental results are from Ljubičić, Nakayama, Isozumi, and Shimizu and the two curves shown represent the predictions of Pisk *et al.* (dashed curve) and the present work (solid curve).

fluence of the nuclear Coulomb field on the electrons in both processes will tend to cancel out. This would lead one to expect the present theory to yield a spectrum for $W_{\mathrm{DIB}}(E,90°)/W_{\mathrm{IB}}(E)$ which has a shape similar to that predicted by the theory of Pisk *et al.* but with an intensity which is reduced by roughly half as much as that experienced by the DIB spectrum itself, and this seems to be borne out by the curves displayed in Fig. 4.

V. CONCLUSIONS

The inclusion of Coulomb effects in the theory of the DIB process leads to a substantial reduction in the overall intensity of the resulting spectra while leaving the shapes of both the two-photon energy spectrum and the sum-energy spectrum largely unchanged. With regard to the sum-energy spectrum, upon comparison with available experimental data one finds some improvement for ^{37}Ar, but there remains a serious disagreement between theory and experiment in the case of ^{55}Fe. For this isotope there is a clear need for further experimental investigation.

To provide a more definitive test of the present theory, there is a need for absolute measurements of the two-photon energy distribution (i.e., relative to the rate for ordinary K capture) or even a similar determination of the sum-energy spectrum. The binding-energy region, in particular, merits such study since it is here that the DIB probability is largest and, at the same time, Coulomb effects are most important. Data taken at angles other than 90° would also be of value.

To study the binding-energy region, it will also be necessary to extend the present theory of the DIB process to include capture from higher shells, specifically from $2s$, $2p$, and $3p$ initial states, since such processes are certain to play an important role at very low energies just as they do in the IB process. And to apply the present theory to this domain, contributions from the second-order amplitude functions will have to be included in the calculations. Thus much work on this process remains to be done, and it is hoped that the present paper will serve to encourage renewed experimental efforts to study this rare but interesting process as well as further theoretical work.

ACKNOWLEDGMENTS

I wish to express my thanks to C.L. Lin and S. Gillespie for reproducing in digitized form the experimental data shown in Figs. 3 and 4 and to E.T. Gawlinski for his advice on computational matters. I have also benefited from many discussions with S.Y. Larsen.

APPENDIX A

In this appendix we illustrate the methods by which the six amplitude functions defined by Eq. (25) can be simplified analytically, thereby reducing the number of integrations for which numerical procedures become necessary. For the purpose of demonstration it is sufficient to consider in detail the reduction of a representative member of the set Λ. The other amplitude functions may be treated in an entirely similar manner; for them only final results will be presented.

For each of the three terms in Eq. (18) for the "outer" Green's function there will be a corresponding contribution to Λ so that we may write

$$\Lambda = \Lambda^{(0)} + \Lambda^{(1)} + \Lambda^{(2)}. \tag{A1}$$

In the following sections we describe in detail the reduction of the amplitude function S_0 to illustrate the methods employed. This is followed by a summary of final results for all the amplitude functions for each of the three orders that contribute.

1. Zero-order amplitude functions

We begin by introducing Eq. (19) for $\widetilde{G}^0_{\mathcal{E}}(\vec{p}_1,\vec{p}_2)$ into Eq. (25) and performing the integration over $\vec{p}_2$, thereby obtaining

$$S_0^{(0)} = -2\int_0^\infty ds\left(\frac{1+s}{s}\right)^\eta \times \int d\vec{p}_1 \frac{1}{(p_1^2-2\mathcal{E})}\frac{1}{(a^2+t_1^2)^2}\frac{1}{(\sigma^2+q_1^2)}, \tag{A2}$$

where $\vec{t}_1 = \vec{p}_1 + \vec{k}_2$ and $\vec{q}_1 = \vec{p}_1 - \vec{k}_1$.

We now make use of Feynman's well-known parametrization technique for replacing a product of momentum-dependent denominators by a single denominator [22] . Specifically, we employ the formula

$$\frac{1}{a^2bc} = 6\int_0^1 dx\int_0^{1-x} dy \frac{(1-x-y)}{[a+(b-a)x+(c-a)y]^4}$$

to rewrite Eq. (A2) as

$$S_0^{(0)} = -12\int_0^\infty ds\left(\frac{1+s}{s}\right)^\eta \times \int_0^1 dx\int_0^{1-x} dy\,(1-x-y) \times \int d\vec{p}_1 \frac{1}{\left[p_1^2 - 2\vec{b}_0\cdot\vec{p}_1 + c_0\right]^4}, \tag{A3}$$

with

$$\vec{b}_0 = x\vec{k}_1 - (1-x-y)\vec{k}_2, \tag{A4a}$$

$$c_0 = (1-x-y)(a^2+k_2^2) - 2y\mathcal{E} + x(\sigma^2+k_1^2). \tag{A4b}$$

The integration over $\vec{p}_1$ may now be performed by simply recalling the following integration formula (valid for $n \geq 2$), which is associated with Feynman's method:

$$\int_{-\infty}^{\infty} \frac{d\vec{k}}{\left(k^2 - 2\vec{k}\cdot\vec{p}+s\right)^n} = \frac{\Gamma(n-3/2)}{\Gamma(n)}\frac{\pi^{3/2}}{(s-p^2)^{n-3/2}}.$$

Its employment in Eq. (A3) leads to

$$S_0^{(0)} = -\frac{3}{2}\pi^2 \int_0^\infty ds \left(\frac{1+s}{s}\right)^\eta \times \int_0^1 dx \int_0^{1-x} dy \frac{(1-x-y)}{(c_0 - b_0^2)^{5/2}}. \quad \text{(A5)}$$

Since further analytic reduction does not appear possible, we conclude our analysis of $S_0^{(0)}$ by preparing Eq. (A5) for numerical evaluation. This simply involves making the change of variable

$$s \to u = s/(1+s),$$

which results in the following final expression for $S_0^{(0)}$:

$$S_0^{(0)} = -\frac{3}{2}\pi^2 \int_0^1 dx \int_0^{1-x} dy \int_0^1 du \frac{u^{-\eta}}{(1-u)^2} \frac{(1-x-y)}{(c_0 - b_0^2)^{5/2}}, \quad \text{(A6)}$$

where c_0 and b_0 are now regarded as functions of x, y, and u.

The reduction of the other zero-order amplitude functions proceeds similarly. The final results for all of them may be summarized as follows:

$$\Lambda^{(0)} = -\frac{3}{2}\pi^2 \int_0^1 du \int_0^1 dx \int_0^{1-x} dy (1-x-y) \frac{u^{-\eta}}{(1-u^2)} \Sigma^{(0)}, \quad \text{(A7)}$$

with the members of the associated zero-order set $\Sigma^{(0)} = \{s_0^{(0)}, s_1^{(0)}, \vec{v}_0^{(0)}, \vec{v}_1^{(0)}, \vec{v}_2^{(0)}, t_{ij}^{(0)}\}$ given by

$$s_0^{(0)} = d_0^{5/2}, \quad \text{(A8a)}$$

$$s_1^{(0)} = 5\sigma x d_0^{7/2}, \quad \text{(A8b)}$$

$$\vec{v}_0^{(0)} = (\vec{b}_0 + \vec{k}_2) d_0^{5/2}, \quad \text{(A8c)}$$

$$\vec{v}_1^{(0)} = 5\sigma x (\vec{b}_0 - \vec{k}_1) d_0^{7/2}, \quad \text{(A8d)}$$

$$\vec{v}_2^{(0)} = 5\sigma x (\vec{b}_0 + \vec{k}_2) d_0^{7/2}, \quad \text{(A8e)}$$

$$t_{ij}^{(0)} = 5\sigma x \left[(b_{0i} b_{0j} - k_{1i} b_{0j} + b_{0i} k_{2j} + k_{1i} k_{2j}) d_0^{7/2} + \delta_{ij} d_0^{5/2}/5 \right], \quad \text{(A8f)}$$

with d_0 defined by $d_0 = 1/(c_0 - b_0^2)$.

2. First-order amplitude functions

The reduction of the first-order contribution to S_0 proceeds largely along similar lines. We begin by introducing Eq. (20) for $\tilde{G}_{\mathcal{E}}^1(\vec{p}_1, \vec{p}_2)$ into Eq. (25), thereby obtaining

$$S_0^{(1)} = -\frac{2\bar{a}}{\pi^2} \int_0^\infty ds \left(\frac{1+s}{s}\right)^\eta \int d\vec{p}_1 \int d\vec{p}_2 \frac{1}{(2\mathcal{E} - p_1^2)} \frac{1}{(2\mathcal{E} - p_2^2)} \frac{1}{(\vec{p}_1 - \vec{p}_2)^2} \frac{1}{(a^2 + q_2^2)^2} \frac{1}{(\sigma^2 + q_1^2)}. \quad \text{(A9)}$$

We again make use of Feynman's parametrization technique, this time employing the formula

$$\frac{1}{a^2 bcd} = 4! \int_0^1 dx \int_0^x dy \int_0^y dz \frac{z}{[az + b(y-z) + c(x-y) + d(1-x)]^5},$$

to rewrite Eq. (A9) as

$$S_0^{(1)} = \frac{48\bar{a}}{\pi^2} \int_0^\infty ds \left(\frac{1+s}{s}\right)^\eta \int_0^1 dx \int_0^x dy \int_0^y dz \int d\vec{p}_1 \int d\vec{p}_2 \frac{1}{(2\mathcal{E} - p_1^2)} \frac{z}{\left[a_1 p_2^2 - 2\vec{b}_1 \cdot \vec{p}_2 + c_1\right]^5}, \quad \text{(A10)}$$

with

$$a_1 = (1 - y + z), \quad \text{(A11a)}$$

$$\vec{b}_1 = (x-y)\vec{p}_1 - z\vec{k}_2, \quad \text{(A11b)}$$

$$c_1 = z(a^2 + k_2^2) + (y-z)(\sigma^2 + q_1^2) + (x-y)p_1^2 - 2\mathcal{E}(1-x). \quad \text{(A11c)}$$

The integration over $\vec{p}_2$ may now be performed with the aid of the Feynman integration formula introduced in the preceding section. Its use in Eq. (A10) leads to

$$S_0^{(1)} = \frac{15\bar{a}}{4}\int_0^\infty ds\left(\frac{1+s}{s}\right)^\eta \int_0^1 dx\int_0^x dy\int_0^y dz\int d\vec{p}_1 \frac{z}{(2\mathcal{E}-p_1^2)}\frac{a_1^2}{(a_1c_1-b_1^2)^{7/2}}. \tag{A12}$$

Next, we introduce spherical coordinates in $\vec{p}_1$ space and perform the angular part of the $\vec{p}_1$ integration using standard methods. The result of this is

$$S_0^{(1)} = 3\pi\bar{a}\int_0^\infty ds\left(\frac{1+s}{s}\right)^\eta \int_0^1 dx\int_0^x dy\int_0^y dz\, z\int_0^\infty dp_1 \frac{p_1}{(2\mathcal{E}-p_1^2)}\frac{a_1^2}{g_i}\left[\frac{1}{(f_i-p_1g_i)^{5/2}}-\frac{1}{(f_i+p_1g_i)^{5/2}}\right], \tag{A13}$$

where

$$d_1 = z(a^2+k_2^2)+(y-z)(\sigma^2+k_1^2)+(x-z)p_1^2-2\mathcal{E}(1-x), \tag{A14a}$$
$$f_1 = a_1d_1-(x-y)^2p_1^2-z^2k_2^2, \tag{A14b}$$
$$\vec{g}_1 = 2z(x-y)\vec{k}_2-2a_1(y-z)\vec{k}_1, \tag{A14c}$$
$$g_1 = (\vec{g}_1\cdot\vec{g}_1)^{1/2}. \tag{A14d}$$

At this point we prepare for numerical integration of the five remaining integrals by introducing the following changes of variable:

$$s\to u = s/(1+s),$$
$$p_1\to v = p_1^2/(1+p_1^2),$$

resulting in the following final expression for $S_0^{(1)}$:

$$S_0^{(1)} = \frac{3}{2}\pi\bar{a}\int_0^1 du\int_0^1 dv\int_0^1 dx\int_0^x dy\int_0^y dz\frac{u^{-\eta}}{(1-u)^2}\frac{z}{(1-v)^2}\frac{1}{(2\mathcal{E}-p_1^2)}\frac{a_1^2}{g_1}\left[\frac{1}{(f_1-p_1g_1)^{5/2}}-\frac{1}{(f_1+p_1g_1)^{5/2}}\right], \tag{A15}$$

in which a_1, g_1, f_1, and p_1 are to be regarded as functions of x, y, z, u, and v.

The reduction of the other first-order amplitude functions proceeds similarly. The final results for all of them are

$$\Lambda^{(1)} = \int_0^1 du\int_0^1 dv\int_0^1 dx\int_0^x dy\int_0^y dz F^{(1)}(x,y,z,u,v)\Sigma^{(1)}, \tag{A16}$$

with the common part of the integrands given by

$$F^{(1)}(x,y,z,u,v) = \frac{15}{2}\pi\bar{a}\frac{u^{-\eta}}{(1-u)^2}\frac{z}{(1-v)^2}\frac{1}{(2\mathcal{E}-p_1^2)}\frac{a_1}{g_1}, \tag{A17}$$

and the members of the associated first-order set $\Sigma^{(1)} = \{s_0^{(1)}, s_1^{(1)}, \vec{v}_0^{(1)}, \vec{v}_1^{(1)}, \vec{v}_2^{(1)}, t_{ij}^{(1)}\}$ given by

$$s_0^{(1)} = a_1I_5^{(1)}/5, \tag{A18a}$$
$$s_1^{(1)} = \sigma a_1^2(y-z)I_7^{(1)}, \tag{A18b}$$
$$\vec{v}_0^{(1)} = \left[(1-y)I_5^{(1)}\vec{k}_2+(x-y)J_5^{(1)}\vec{g}_1\right]/5, \tag{A18c}$$
$$\vec{v}_1^{(1)} = \sigma a_1^2(y-z)\left[J_7^{(1)}\vec{g}_1-I_7^{(1)}\vec{k}_1\right], \tag{A18d}$$
$$\vec{v}_2^{(1)} = \sigma a_1(y-z)\left[(1-y)I_7^{(1)}\vec{k}_2+(x-y)J_7^{(1)}\vec{g}_1\right], \tag{A18e}$$
$$t_{ij}^{(1)} = \sigma a_1(y-z)\Bigg[(1-y)J_7^{(1)}g_{1i}k_{2j}-(x-y)\times J_7^{(1)}k_{1i}g_{1j}-(1-y)I_7^{(1)}k_{1i}k_{2j}+(x-y)\left\{K_3^{(1)}g_{1i}g_{1j}/g_1^2-K_2^{(1)}\delta_{ij}/3\right\}\Bigg], \tag{A18f}$$

in which we have employed the following definitions with $i = 1$:

$$I_n^{(i)} = \left[\frac{1}{(f_i-p_1g_i)^{n/2}}-\frac{1}{(f_i+p_1g_i)^{n/2}}\right], \tag{A19a}$$
$$J_n^{(i)} = \frac{1}{(n-2)g_i^2}\left[\frac{(2f_i-np_1g_i)}{(f_i-p_1g_i)^{n/2}}-\frac{(2f_i+np_1g_i)}{(f_i+p_1g_i)^{n/2}}\right], \tag{A19b}$$
$$K_n^{(i)} = \frac{1}{5g_i^2}\left[\frac{(4f_i^2-14f_ip_1g_i+n5p_1^2g_i^2)}{(f_i-p_1g_i)^{7/2}}-\frac{(4f_i^2+14f_ip_1g_i+n5p_1^2g_i^2)}{(f_i+p_1g_i)^{7/2}}\right]. \tag{A19c}$$

3. Second-order amplitude functions

The procedure for reducing the second-order contributions to the amplitude functions is identical to that used to simplify the first-order contributions. The final results are of the same form, except for one additional integration, and differ only in a few details. Thus we present only final results, prefaced by the following set of definitions:

$$a_2 = a_1 + (x-y)(2\mathcal{E} - p_1^2)(1-\rho)^2/8\rho\mathcal{E}, \tag{A20a}$$

$$d_2 = d_1 - (x-y)(2\mathcal{E} - p_1^2)(1-\rho)^2/4\rho, \tag{A20b}$$

$$f_2 = a_2 d_2 - (x-y)^2 p_1^2 - z^2 k_2^2, \tag{A20c}$$

$$\vec{g}_2 = 2z(x-y)\vec{k}_2 - 2a_2(y-z)\vec{k}_1, \tag{A20d}$$

$$g_2 = (\vec{g}_2 \cdot \vec{g}_2)^{1/2}, \tag{A20e}$$

with which the second-order amplitude functions may be written as:

$$\Lambda^{(2)} = \int_0^1 du \int_0^1 dv \int_0^1 d\rho \int_0^1 dx \int_0^x dy \int_0^y dz F^{(2)}(x,y,z,u,v,\rho)\Sigma^{(2)}, \tag{A21}$$

with the common part of the integrands given by

$$F^{(2)}(x,y,z,u,v,\rho) = \frac{15}{2}\pi\bar{a}\nu \frac{u^{-\eta}}{(1-u)^2}\frac{z}{(1-v)^2}\frac{\rho^{-\nu-1}}{(2\mathcal{E}-p_1^2)}\frac{a_2}{g_2}, \tag{A22}$$

and the members of the associated second-order set $\Sigma^{(2)} = \{s_0^{(2)}, s_1^{(2)}, \vec{v}_0^{(2)}, \vec{v}_1^{(2)}, \vec{v}_2^{(2)}, t_{ij}^{(2)}\}$ given by

$$s_0^{(2)} = a_2 I_5^{(2)}/5, \tag{A23a}$$

$$s_1^{(2)} = \sigma a_2^2 (y-z) I_7^{(2)}, \tag{A23b}$$

$$\vec{v}_0^{(2)} = \left[(a_2 - z)I_5^{(2)}\vec{k}_2 + (x-y)J_5^{(2)}\vec{g}_2\right]/5, \tag{A23c}$$

$$\vec{v}_1^{(2)} = \sigma a_2^2 (y-z)\left[J_7^{(2)}\vec{g}_2 - I_7^{(2)}\vec{k}_1\right], \tag{A23d}$$

$$\vec{v}_2^{(2)} = \sigma a_2 (y-z)\left[(a_2 - z)I_7^{(2)}\vec{k}_2 + (x-y)J_7^{(2)}\vec{g}_1\right], \tag{A23e}$$

$$t_{ij}^{(2)} = \sigma a_2 (y-z)\left[(a_2-z)J_7^{(2)}g_{2i}k_{2j} - (x-y)\,J_7^{(2)}k_{1i}g_{2j} - (a_2-z)I_7^{(2)}k_{1i}k_{2j} + (x-y)\left\{K_3^{(2)}g_{2i}g_{2j}/g_2^2 - K_2^{(2)}\delta_{ij}/3\right\}\right], \tag{A23f}$$

in which we have employed Eqs. (A19) with $i = 2$.

APPENDIX B

Here we record for ease of reference two well-known formulas [5] that we use in the evaluation and plotting of our final results. For normalization purposes we employ the transition rate for ordinary allowed K capture which, in the nonrelativistic Coulomb approximation, is given by

$$W_K = 2G^2\frac{a^3}{\pi^2}k_{\max}^2 BB^*, \tag{B1}$$

where, as before, we have assumed the presence of two K electrons initially.

Within the same nonrelativistic Coulomb approximation that we have used for our study of the DIB process, the transition rate for IB during an allowed K-capture transition is given by the following formula due to Glauber and Martin [3]:

$$dw_\gamma = W_K \frac{\alpha}{(2\pi)^2} k\,(1 - k/k_{\max})^2 \frac{(1+B_{1s}^2)}{2} dk d\Omega, \tag{B2}$$

with

$$B_{1s}(k) = 1 - \frac{4}{3}\frac{\eta_1}{(1+\eta_1)}\left[1 + \frac{\eta_1}{(1-\eta_1)}\{2K(\lambda_1) - 1\}\right], \tag{B3}$$

and $\lambda_1 = (1-\eta_1)/(1+\eta_1)$, $\eta_1 = (1 + k/B_K)^{-1/2}$, where B_K is the K-shell binding energy, and $K(\lambda_1)$ is represented by

$$K(\lambda_1) = \lambda_1 \int_0^1 \frac{dx\, x^{-\eta_1}}{(1+\lambda_1 x)} = \ln(1+\lambda_1) - \eta_1 \sum_{n=1}^{\infty} \frac{(-\lambda_1)^n}{n(n-\eta_1)}. \tag{B4}$$

[1] C. Möller, Phys. Z. Sowjetunion **11**, 9 (1937).
[2] P. Morrison and L. I. Schiff, Phys. Rev. **58**, 24 (1940).
[3] R. J. Glauber and P. C. Martin, Phys. Rev. **104**, 158 (1956).
[4] P. C. Martin and R. J. Glauber, Phys. Rev. **109**, 1307 (1958).
[5] W. Bambynek, H. Behrens, M. H. Chen, B. Crasemann, M. L. Fitzpatrick, K. W. D. Ledingham, H. Genz, M. Mutterer, and R. L. Intemann, Rev. Mod. Phys. **49**, 77 (1977).
[6] A. Ljubičić, R. T. Jones, and B. A. Logan, Nucl. Phys. **A236**, 158 (1974).

[7] K. Pisk, A. Ljubičić, and B. A. Logan, Nucl. Phys. **A267**, 77 (1976).
[8] B. A. Logan, A. Ljubičić, K. Pisk, and Z. Roller-Ivanović, Phys. Rev. C **16**, 2078 (1977).
[9] A. Ljubičić, Y. Nakayama, Y. Isozumi, and S. Shimizu, Nucl. Phys. **A320**, 289 (1979).
[10] J. Dobrinić, N. Orlić, S. Kaučić, D. Kerez, A. Ljubičić, and B. A. Logan, Nucl. Instrum. Methods Phys. Res. Sect. A **280**, 384 (1989).
[11] N. Orlić, S. Kaučić, A. Ljubičić, K. Pisk, and B. A. Logan, Nucl. Phys. **A433**, 397 (1985).
[12] Z. Roller, K. Pisk, and A. Ljubičić, Nucl. Phys. **A390**, 43 (1982).
[13] K. Pisk, V. Pašagić, and B. A. Logan, Nucl. Phys. **A433**, 383 (1985).
[14] We employ units in which $m = c = \hbar = 1$ (m is the electron mass), $e^2/4\pi = \alpha \approx 1/137$. $x_\mu = (\vec{r}, it)$ and the Dirac matrices are defined by $\vec{\gamma} = -i\beta\vec{\alpha}$ and $\gamma_4 = \beta$. Also $\gamma_5 = \gamma_1\gamma_2\gamma_3\gamma_4$ and $\bar{\phi} = \phi^\dagger\gamma_4$.
[15] This form assumes the use of a Green's function which is nonsingular at $r_n = 0$.
[16] Here we are assuming that the energy released in the electron-capture transition is below the threshold at which competing positron emission becomes possible. In this case the Green's function decreases rapidly with distance from the nucleus and has a range which depends on k_1 and k_2.
[17] We also have assumed that the initial nucleus is unpolarized and that the spin state of the final nucleus is unobserved.
[18] J. Schwinger, J. Math. Phys. **5**, 1606 (1964).
[19] W. H. Press, S. A. Teukolsky, W. T. Vetterling, and B. P. Flannery, *Numerical Recipes in FORTRAN: the Art of Scientific Computing* (Cambridge University Press, New York, 1992), pp. 309–314.
[20] A similar effect is known to occur in the IB process. See, for example, Fig. 34 of Ref. [5].
[21] The relations are those described by Eqs. (10) and (11) of Pisk *et al.* after being transformed to variables more suitable for numerical integration. They have been used to reconstruct the theoretical results of Pisk *et al.* as well as to construct the results of the present theory.
[22] J. M. Jauch and F. Rohrlich, *The Theory of Photons and Electrons* (Springer-Verlag, New York, 1976), Appendix 5A.